PHILOSOPHICAL TRANSACTIONS A

royalsocietypublishing.org/journal/rsta

Research

Cite this article: Kumar P, Benzi R, Trampert J, Toschi F. 2020 A multi-component lattice Boltzmann approach to study the causality of plastic events. *Phil. Trans. R. Soc. A* **378**: 20190403.
http://dx.doi.org/10.1098/rsta.2019.0403

Accepted: 11 May 2020

One contribution of 15 to a theme issue 'Fluid dynamics, soft matter and complex systems: recent results and new methods'.

Subject Areas:
statistical physics, geophysics, fluid mechanics

Keywords:
causality, aftershock, earthquake, vibration-induced stabilization, lattice Boltzmann method

Author for correspondence:
Federico Toschi
e-mail: f.toschi@tue.nl

Electronic supplementary material is available online at https://doi.org/10.6084/m9.figshare.c.5007299.

THE ROYAL SOCIETY PUBLISHING

A multi-component lattice Boltzmann approach to study the causality of plastic events

Pinaki Kumar[1], Roberto Benzi[2], Jeannot Trampert[3] and Federico Toschi[1]

[1]Department of Applied Physics, Eindhoven University of Technology, PO Box 513, 5600 MB Eindhoven, The Netherlands
[2]Dipartimento di Fisica, Università di Roma 'Tor Vergata' and INFN, Via della Ricerca Scientifica, 1-00133 Roma, Italy
[3]Department of Earth Sciences, Utrecht University, PO Box 80115, NL-3508 TC, Utrecht, The Netherlands

PK, 0000-0001-5026-3261; FT, 0000-0001-5935-2332

Using a multi-component lattice Boltzmann (LB) model, we perform fluid kinetic simulations of confined and concentrated emulsions. The system presents the phenomenology of soft-glassy materials, including a Herschel–Bulkley rheology, yield stress, ageing and long relaxation time scales. Shearing the emulsion in a Couette cell below the yield stress results in plastic topological re-arrangement events which follow established empirical seismic statistical scaling laws, making this system a good candidate to study the physics of earthquakes. One characteristic of this model is the tendency for events to occur in avalanche clusters, with larger events, triggering subsequent re-arrangements. While seismologists have developed statistical tools to study correlations between events, a process to confirm causality remains elusive. We present here, a modification to our LB model, involving small, fast vibrations applied to individual droplets, effectively a macroscopic forcing, which results in the arrest of the topological plastic re-arrangements. This technique provides an excellent tool for identifying causality in plastic event clusters by examining the evolution of the dynamics after 'stopping' an event, and then checking which subsequent events disappear.

This article is part of the theme issue 'Fluid dynamics, soft matter and complex systems: recent results and new methods'.

1. Introduction

Physical systems governed by stick-slip dynamics often display avalanches. Regardless of the nature of these system, they are characterized by similar statistics [1,2]. Many events within an avalanche trigger subsequent events. In seismology, for instance, a large earthquake is classified as the *main-shock* while subsequent smaller events occurring nearby, and thus believed to be triggered by the main-shock, are classified as *aftershocks*. The time decay of aftershock frequency following a main-shock is captured in the celebrated empirical Omori's Law [3], but numerous other systems display this time decay [2].

While the term aftershock might imply ascertained causality between earthquake event pairs, the seismologic literature is ambiguous and unsettled as to its definition. Attempts at classifying aftershocks in earthquake catalogues have relied on simple space–time windowing approaches [4,5]; single-link graphs based on a distance metric [6]; a context-dependent game-theoretic combination of above methods [7]; evolving random graphs based on windowing [8,9]; and a pair-wise nearest-neighbour rescaled space–time-magnitude metric derived from phenomenological laws [10]. The latter was refined [11] to include a threshold separating strongly correlated and background events, which emerged from the bimodal distribution of the nearest-neighbour metric and has since been applied in numerous studies [12–16] with some variations.

It is to be noted that all the above-mentioned tools are in fact statistical, which simply try to assign a correlation between the events, with causality itself being assumed to be valid above some prescribed threshold in the correlation. This inability to firmly establish causality is, of course, understandable, given that seismologists do not have access to a real-time dynamical state of stress or accurate microscopic knowledge of earthquake nucleation sites inside the Earth. However, a proxy earthquake analogue [17] based on numerical simulations of soft glasses, with access to the relevant dynamic variables at all scales, in theory, does not suffer such limitations. We propose here to develop an objective causality criterion for such a system, which, for instance, could serve to benchmark statistical tools in seismology based on correlations.

We, therefore, turn our attention to this recently introduced model, based on a mesoscopic lattice Boltzmann (LB) description for a mixture of non-ideal binary fluids, stabilized from coarsening via frustration effects at the interface [18]. A very brief summary of the model follows; for more details see [17,18]. On a regular two-dimensional lattice for each fluid species, the probability of finding a particle at position r at time t is given by the distribution function, $f_i(r, c_i; t)$. Here, c_i is the discrete velocity, with index i, running over nearest and next-to-nearest neighbours of r. The time evolution of f_i towards a local equilibrium f_i^{eq} is given by

$$f_i(r + c_i, c_i; t + 1) = f_i(r, c_i; t) - \frac{1}{\tau_{lb}}(f_i - f_i^{\mathrm{eq}})(r, c_i; t) + F_i(r, c_i; t), \tag{1.1}$$

where τ_{lb} is a characteristic time scale and F_i represents inter-particle forcing, which includes inter-species repulsion, short-range intra-species attraction and long-range repulsion. Simulations of droplets of the two fluids under external shear (Couette cell), with one dispersed in the other at a high packing fraction using these simple internal forcing rules, lead to highly non-trivial emergent dynamics, like a finite yield-stress (σ_y) and a Herschel–Bulkley rheology [19]. When sheared below σ_y, sudden and highly intermittent T1 topological re-arrangements (plastic events) involving four droplets (quartets) are observed (figure 1*a*), coinciding with stress drops (figure 1*b*), which radiate energy via elastic waves [20]. The intermittency and statistical properties of these activity bursts can be observed by defining a suitable measure of displacement $\mathcal{A}_i$, a two-dimensional scalar field, which is simply the difference of the squared density field across consecutive time steps per sub-box i into which the domain is divided, the supremum of which, A_{sup}, is shown in figure 1*b*. The square root of A_{sup} is proportional to the seismic moment [17] and follows established empirical earthquake scaling laws. Together with its clear stick-slip behaviour, scaling properties of inter-avalanche waiting times, multi-fractal appearance of event locations

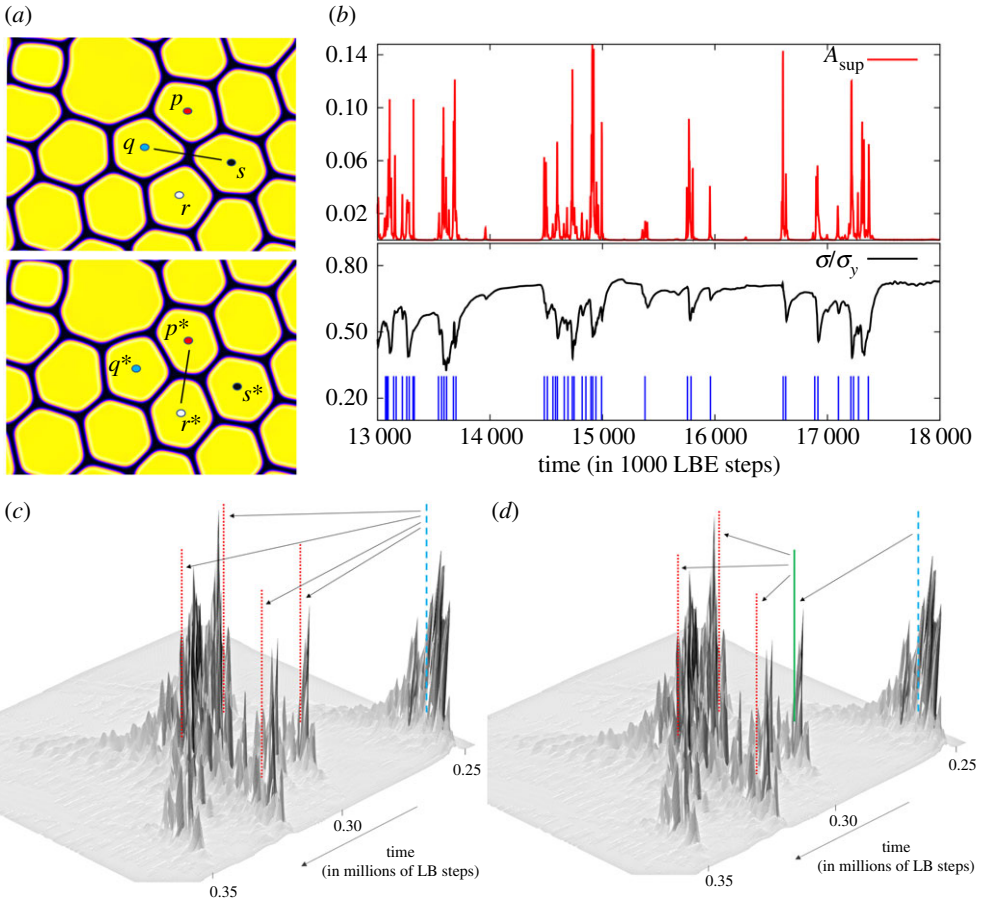

Figure 1. (*a*) Density field of our binary fluid soft-glass undergoing a plastic topological re-arrangement event where nearest neighbours (q, s) (top panel) switch over to (p^*, r^*). (*b*) A snapshot of the supremum of the two-dimensional scalar displacement, A_{sup} (top panel) and the normalized shear stress (lower panel), for the same duration are plotted. The spikes in the lower panel indicate discrete detections of plastic events. (*c*,*d*) The figures shows a projection of the scalar displacement field $\mathcal{A}_i$ along the x-axis as a function of y and time. The superimposed lines indicate individual plastic events. The space–time clustering of events into avalanches is clearly apparent. Two hypothetical scenarios regarding causal triggering of events are presented. (*c*) A single (dashed) event triggers all the other (dotted) events. (*d*) The single (dashed) event triggers just one (solid) event, which in turn causes the rest (dotted). (Online version in colour.)

among several other characteristics [2], make this system an interesting proxy to study earthquake physics. These results do not depend on the use of A_{sup}, as other measures of displacement lead to the same scaling laws in the system [21].

In figure 1*c*,*d*, we show a cluster of events, using the scalar field $\mathcal{A}_i$. The discrete events (biggest spikes) are indicated with lines (solid, dotted, dashed), with perturbations in their neighbourhood clearly visible, radiating out from said events. Two out of several possible causal chains are illustrated (with arrows) and even with access to every relevant dynamical variable, it is difficult to ascertain which chain happens to be true. This is because, physically, there is a highly complex propagation of the disturbance itself (mostly through the interface), compounded further by the interaction of the propagation front with neighbourhood droplets. A possible way forward is offered by recent studies [22–24] which propose, so-called soft spots in disordered glasses, either obtained through vibrational mode analysis or machine-learning techniques and which can a priori identify locations of high non-affine displacement potential, i.e. possible plastic

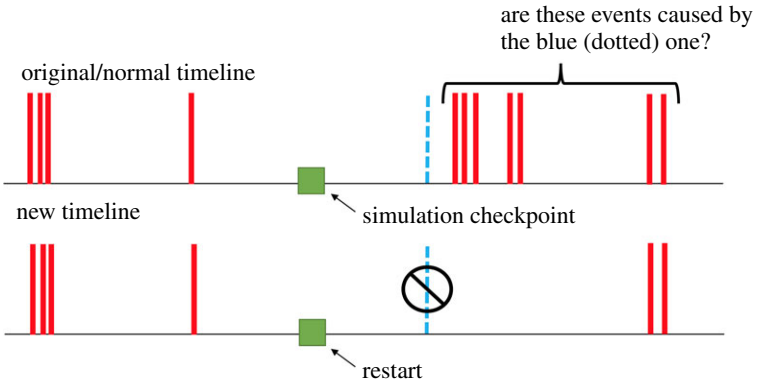

Figure 2. The figure illustrates the idea for inferring causality between a main-shock and its corresponding triggered after-shocks. The solid (red) spikes denote individual plastic events. In a first pass, we run a typical simulation and identify all the plastic events. In a second pass, we re-run the simulation, from a check-point prior to a given plastic event (dashed blue), and if we can hypothetically prevent this blue event from happening, any subsequent events which disappear from the timeline can be confirmed as having been triggered by the blue one. (Online version in colour.)

event spots, by simply looking at the local structure. In our case, this would imply being able to keep a running tally of soft-spots as the propagating perturbations from a prior event affect droplet geometries, resulting in a continuously updated gradation of droplet quartets ordered by 'softness'. Combined with the reasonable assumptions that the weakest spots break first, this would allow a clear establishment of causal chains. However, the cited studies were performed for glasses comprising spheres, and the complex geometries of our droplets make this approach highly non-trivial to adapt.

Instead, our key idea for establishing causality is sketched in the illustration shown in figure 2. Essentially, we wish to create a new timeline of events where we stop a plastic event from occurring and then look to see which subsequent events disappeared. This allows the problem to be reduced to the following: How do we stop a plastic event gracefully, without affecting the neighbouring droplet topology?

2. Arresting plastic events with vibration-induced stabilization

We start by reporting negative results from two rather naive approaches to arresting plastic re-arrangements. The first involves imposing wall boundary conditions enclosing the droplet quartet after simulation restart (prior to the targeted plastic event), whereas in the second case we copied the LB equilibrium populations, f_i^{eq}, corresponding to the lattice sites belonging to the quartet (figure 3*c*) before the plastic event, into a separate buffer (called $f_i^{\mathrm{eq-FRZ}}$) and simply copying it back after each LB time-step update following equation (1.1), in effect, simply pausing LB updates at those lattice sites. In both cases, a disruption to the diffusion current along the interface [18] resulted in strongly accelerated droplet coarsening and eventually destroyed the system topology rendering it inadmissible as an earthquake analogue.

However, progress can be made by taking hints from the ideas of 'soft-spots' outlined earlier [24] and the shear transformation zone theory [25,26], in that we start to view our soft-glass domain through a potential energy landscape perspective. Since plastic events are one of the ways the system dissipates energy (with energy input being constant via the shearing at the walls), it is not unreasonable to state that there is a local potential hill near a spot susceptible to re-arranging, and after the event the hill disappears. So, in theory, all that is needed is to invent a complex body force which lowers this potential hill or, in other words, makes an unstable configuration stable or, at least, metastable.

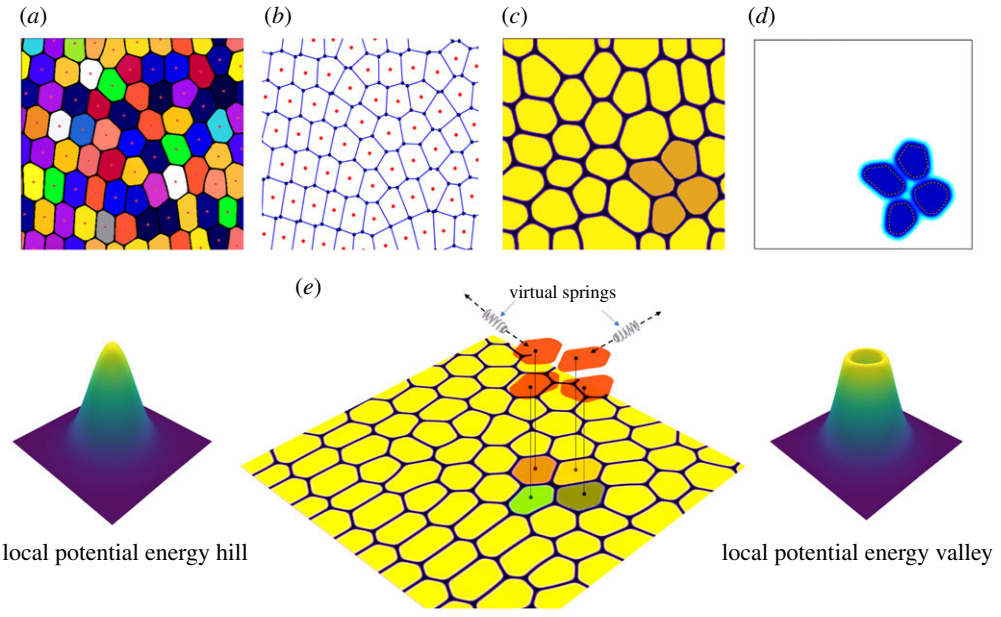

Figure 3. (*a*) Colouring of the thresholded density field using the flood-fill algorithm. Dots represent centres of mass. (*b*) Radical Voronoi tessellation to detect plastic events. (*c*) Identifying the droplets involved and selecting corresponding 'pixels' for stencil. (*d*) Smoothening and visualization of the final stencil geometry. (*e*) Next, the stencil from part (*d*) is modulated in time following equation (2.1), with equation (2.2) providing the modified LB update scheme. This results in an oscillatory motion of the four droplets along the axes shown (dotted arrows) which passes through the collective centre of mass. This, in our case, is the analogue for the Kapitza vibrating pendulum, which turns a local potential energy hill (covering the droplet quartet) into a valley, thus gracefully stopping the event. (Online version in colour.)

The search for such a hypothetical forcing scheme is readily addressed by taking inspiration from the classical problem of stabilization of an inverted pendulum on a vibrating base [27]. First proposed by Kapitza and later generalized by Landau [28], the method of separation of forces tells us that small-amplitude, high-frequency periodic forcing acting on a particle moving through a potential field can be substituted by an effective force, and with a tuning of the vibratory force parameters the particle can be trapped in a potential valley. This stabilization technique has been adapted and found extensive use in a variety of applications such as an explanation for the Indian magic rope trick [29], the phenomena of droplet levitation on a vibrating base [30], formation of stable shear-banding behaviour in a soft-glass [31], etc.

To adapt this technique to our case, first we needed to precisely isolate the target droplet quartet geometry (figure 3*a–d*) as it will be discussed later. Then, the displacement bounds of the droplets induced by the vibratory forcing were to be determined. This too necessitated some care in selection, since the approach calls for small-amplitude vibrations and, also, since increasing amplitudes would increase the risk of non-local effects. So, a quiescent period, slightly before the event is to occur, is chosen and the LB equilibrium population distributions corresponding to the quartet lattice sites is stored in a separate buffer, called $f_i^{\mathrm{eq-FRZ}}$. These stored populations represent one extremum of the displacement bound, with the other bound emerging from the quartet's tendency to deform and re-arrange, the extent of the re-arrangement allowed being set parametrically by the periodic time function of the vibratory forcing. Or to put it more simply, we are forcing the droplets to vibrate between the static configuration prior to the event and a parametrically controlled 'partial' re-arrangement (i.e. an elastic re-arrangement in contrast to the usual plastic mode). The idea is sketched in the illustration shown in figure 3*e*, where this periodic partial re-arrangement is imagined by putting a virtual spring, forcing the droplets along an axis connecting their individual centres of mass and the collective centre of mass for the quartet.

We now briefly touch upon the actual technical modalities associated with carrying out the outlined process. Starting with geometry extraction, we draw heavily from image processing literature and the following steps were followed.

(i) The density field of a fluid component is thresholded [32] to obtain a binary image with '1s' representing the droplet bulk and '0s' for the interface.
(ii) Random labels are scattered on a uniform grid covering the domain, which act as seeds for the flood-fill algorithm [33] performed recursively for each droplet, until every droplet has been assigned an unique label (figure 3*a*). Next, for each droplet, since we know all its constituent pixels (lattice sites), we can compute the centre of mass.
(i) This is followed by a radical Voronoi tessellation (figure 3*b*) which can be thought of as just a weighted version of the standard Voronoi algorithm [34], to give us the interface topology and droplet neighbour connectivity. For each time step, this connectivity information along with the details identified in step (ii) are stored in a graph database like *networkx* [35].
(iii) Once steps (i)–(iii) have been performed for every time step in a simulation, all plastic events with the droplet quartets involved in the event are identified by comparing tessellations across time steps and looking at changing edge counts.
(iv) The pixels corresponding to the re-arranging quartet identified in step (iv) are extracted from the 'coloured' array obtained from step (ii) (figure 3*c*) and used to make a binary stencil (with the quartet being labelled 1 and every other droplet, labelled 0).
(ii) Finally, the sharp stencil is smoothed using a simple two-dimensional diffusion schema, $\frac{\partial T(r,t)}{\partial t} = D\nabla^2 T(r,t)$ (figure 3*d*). The extent of smoothing is empirically identified and roughly equals the width of the interface.

Next, we formulate our temporal function as in equation (2.1).

$$g(t) = \lambda\left[\tanh\left(\frac{t^* - T_{\text{start}}}{t_w}\right) - \tanh\left(\frac{t^* - T_{\text{end}}}{t_w}\right)\right], \tag{2.1}$$

where λ is an amplitude, $t^* = t \mod T_{\text{cycle}}$ with T_{cycle} representing the cycle duration (in LB units), and T_{start}, T_{end} and t_w are simply tunable parameters to control the shape of the vibratory waveform. We note here that this form of periodic function was only to achieve finer control of the tuning process, and is not a necessity. Empirically, we observe that the only condition that seems necessary is that the periodic function be smooth, i.e. continuously differentiable, thus, for example $|\sin(t)|$ is not effective.

We then combine our temporal function, $g(t)$, and our spatial stencil of the droplet geometry, into a spatio-temporal field, that we denote $\epsilon(x, y; t)$. Finally, we take the equilibrium population distribution of the system prior to the plastic event, $f_i^{\text{eq}-\text{FRZ}}$, and modify the LB update scheme of equation (1.1) as follows:

$$f_i^* = (1-\epsilon)\underbrace{\left(f_i - \frac{1}{\tau}(f_i - f_i^{\text{eq}}) + F_i\right)}_{\text{normal LB update}} + \epsilon(f_i^{\text{eq}-\text{FRZ}}). \tag{2.2}$$

3. Results

We perform numerical simulations on a small 256^2 domain (approx. 40 droplets) for visual validation purposes and can confirm that the effectiveness of the method is independent of the system size. Since static images of the density field are ill suited for demonstration of topological arrest (movies of the density field corresponding to figure 4 are uploaded as electronic supplementary material), we resort to showing the shear stress as a proxy for plastic activity as we alluded to previously in figure 1*b*. We illustrate our results with a sample case study as shown in figure 4. The dotted (red) line shows the stress time behaviour for a normal simulation with a

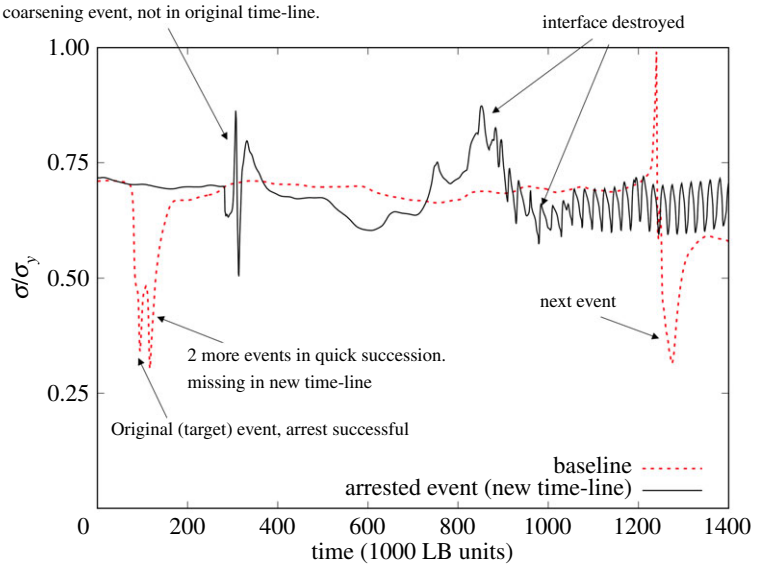

Figure 4. Stress–time evolution of the system under a normal baseline scenario (shown with dotted red line) and a case where a plastic event is stopped (shown with a solid black line). The stress drops associated with an event can be seen to vanish in the arrested scenario. Furthermore, not only is the original event stopped but subsequent events disappear, thus implying causality. (Online version in colour.)

stress drop at roughly the 100 K time mark and two distinct dips. The first dip is a single plastic event and is our target for arrest while the second dip is in fact two events occurring in rapid succession. We note here that plastic events occur on a small but finite time duration of about 5000 time steps.

The solid line (black) line represents a simulation re-started from a checkpoint prior to the target event and a successful arrest of said event (no stress drop). Furthermore, not only is the targeted event stopped but also the two subsequent events disappear in this new timeline. This provides strong evidence of a causal link between the stopped event and the ones that disappeared afterwards.

Looking further in figure 4, we see a spike in the new timeline at about 250 K which is absent from the original timeline. This spike is not a plastic event but rather a small coarsening event, where a droplet overcomes the dis-joining pressure at the interface and merges with another. Though this coarsening involved a small droplet (compared to the mean size), occurred far away (several droplet diameters away) from the target site and we have cases which lack such 'novelty' in the new timeline on shorter time scales, we show it to emphasize that this paradigm for causality detection is valid, as long as the simulation dynamic evolution does not change prior to the targeted event. This means, for example, a separate 'new' event occurring after simulation re-start in figure 2 before the dotted (blue) event or the droplet coarsening event in figure 4 happening before the initial targeted event in the original timeline. Such cases of novelty in the new timeline would render the arrest pointless.

Here, we bring up the relevant time scales for this topological arrest exercise. The elastic wave radiating from an event, which we believe to be the cause for triggering other events, not dissimilar to the P and S waves seen in real earthquakes, travels at a finite speed [20] and we will call the time it takes for this wave to travel from the event site to the farthest point in the domain as τ_c which, for our case of a 256^2 domain, $\tau_c \approx 14300$ LB time steps. These elastic waves dissipate due to viscosity over time and, empirically, a time duration of $15\tau_c$ seems to be the point after which we can say with relative certainty that events triggered after this point in time are independent and random.

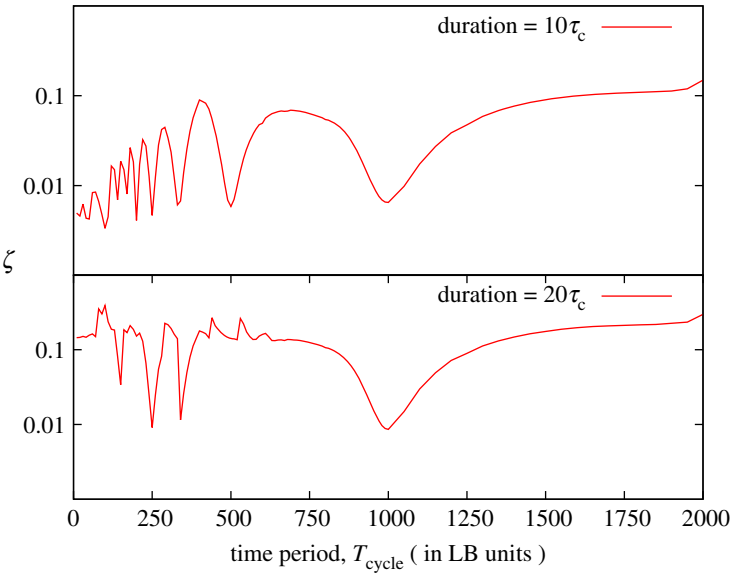

Figure 5. The metric for assessing arrest quality, ζ (equation (3.1)), is plotted for a range of time periods, T_{cycle} from equation (2.1) and for two arrest durations. A lower value of ζ indicates better arrest and less collateral disruption to the system. (Online version in colour.)

The eventual destruction of the interface given sufficient time is almost certain, as in figure 4 starting at the 800 K mark, since plastic events provide the mechanism for relaxation in a system where there is constant pumping of energy via shear at the walls. It stands to reason that after the system has exhausted probing every 'soft' spot, somewhere the desire to relax will overcome the dis-joining pressure maintained by frustration effects at the interface and trigger a cascade of coarsening (figure 4 after the 1000 K mark).

Next, to investigate whether there are optimal vibration parameters, which would allow us to stop events without damaging the system for longer durations (up to ideally longer than $15\tau_c$), we performed a sweep over a range of time periods T_{cycle}. To quantify the quality of the arrests, we define the metric ζ as

$$\zeta = \sum \mathcal{A}_i(t)_{\text{arrested}} / \sum \mathcal{A}_i(t)_{\text{baseline}}. \tag{3.1}$$

Effectively, ζ captures the total relative displacement, $\mathcal{A}_i$, compared to the baseline, over the length of the simulation and for the full domain and includes both plastic events, coarsening events and possible cases of interface destruction. Thus small values of ζ would indicate perfect arrests and minimal disruption and vice versa for higher values. In figure 5, we plot ζ for the same system as in figure 4 for two arrest durations of $10\tau_c$ and $20\tau_c$, respectively.

It seems to be the case that this arrest operation indeed appears to be optimal at certain specific frequencies. From observation of the associated videos of the density field, a value of $\zeta \sim 10^{-2}$ is representative of a very good arrest. For shorter time scales, this seems to be achieved at several values of T_{cycle} while only a few values emerge for longer durations. The amplitude of the vibration, i.e. λ in equation (2.1), was fixed at 0.075 for the time period sweep shown in figure 5 and seems to be the upper-bound of permissible amplitudes. However, preliminary results suggest that lowering the amplitude does not meaningfully affect the optimal time periods, in contrast to the case of the inverted pendulum, where both the amplitude and frequency occur together in the expression for the stable regime of vibration. We note here that, unlike the case of the inverted pendulum, where the range of stabilizing parameters were derived analytically, the current discussion is rather empirical and we aim to investigate this behaviour more rigorously in the future. The longer freezing duration enabled by these choices of parameters allows us to

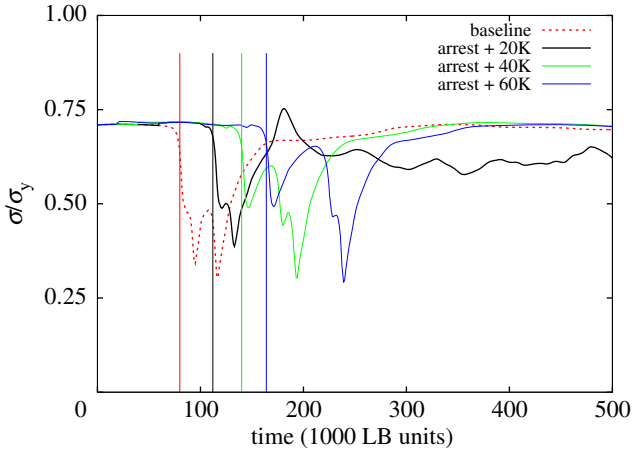

Figure 6. Stress–time evolution of a baseline simulation is shown by the dotted (red) line, while solid line curves indicate simulations where the plastic event is delayed by arrest and subsequent release for the same event as shown in figure 4. The vertical spikes show the times of the discrete event. (Online version in colour.)

gather better statistics on causally linked and equally importantly, independent events, i.e. those events which occurred at the same time and place irrespective of whether a plastic event was priorly stopped or not.

Finally, in figure 6, we show the arrest and subsequent 'release' of the same plastic event as shown in figure 4, whereby releasing implies simply stopping LB update following equation (2.2) and reverting to equation (1.1). The droplet quartet is released after increasing times spent arrested and satisfyingly the original event immediately occurs after release. More interestingly, the two subsequent events from the original timeline also occur following the release of the target event in the cases of +40K and +60K, while a new event at different location follows the target in the case of +20K. The latter is perhaps an artefact from the abruptness of release (for which no thermalization of the forcing was performed unlike in the case of arrest) which was implemented non-ideally in the code. We also like to point out that the coarsening event in the new timeline of figure 4 is absent in figure 6, which supports our earlier assertion that the absence of soft spots barring the one which is arrested, would eventually lead to coarsening and disruption of the interface due to the inability of the system to release energy. Since in figure 6, the target quartet was released from arrest, the need for such coarsening disappeared.

4. Conclusion

In conclusion, a novel way to manipulate plastic topological re-arrangements in a soft-glass seismic analogue has been presented. The intractable problem of inferring causal chains between these plastic events is addressed through an elegant application of the method of separation of forces which allows us to examine dynamic evolution changes in a new-time after the arrest of an event. We are in the process of collecting a database of causally related and random events using our LB model. The present work thus has direct applications in evaluating the accuracy and elucidating the mechanisms underlying the various schemes proposed in the seismic literature which aim to classify earthquake sequences into main-shocks and aftershocks. Furthermore, we are hopeful that this technique can be adapted to experimental studies on soft-glasses, many of which exhibit plastic event phenomenology to varying extents with tools such as optical tweezers used to probe micro-emulsions and ultrasounds applied to granular media.

Data accessibility. The datasets supporting this article have been uploaded as part of the electronic supplementary material.

Authors' contributions. P.K. performed the simulations, data analysis and drafted the manuscript. R.B. and J.T. conceived the project and helped draft the manuscript. F.T. conceived the project, and helped with the data analysis, coding and drafting the manuscript. All authors read and approved the manuscript.

Competing interests. The authors declare that they have no competing interests.

Funding. This research was partly funded by the Shell-NWO/FOM programme 'Computational sciences for energy research' under project no. 14CSER022.

Acknowledgements. Numerical simulations for this work was carried out on the Dutch national e-infrastructure with the support of SURF Cooperative.

References

1. Uhl JT *et al.* 2015 Universal quake statistics: from compressed nanocrystals to earthquakes. *Sci. Rep.* **5**, 16493. (doi:10.1038/srep16493)
2. Kumar P, Korkolis E, Benzi R, Denisov D, Niemeijer A, Schall P, Toschi F, Trampert J. 2020 On interevent time distributions of avalanche dynamics. *Sci. Rep.* **10**, 1–11.
3. Utsu T, Ogata Y *et al.* 1995 The centenary of the Omori formula for a decay law of aftershock activity. *J. Phys. Earth* **43**, 1–33. (doi:10.4294/jpe1952.43.1)
4. Gardner J, Knopoff L. 1974 Is the sequence of earthquakes in Southern California, with aftershocks removed, Poissonian? *Bull. Seismol. Soc. Am.* **64**, 1363–1367.
5. Knopoff L, Kagan Y, Knopoff R. 1982 b Values for foreshocks and aftershocks in real and simulated earthquake sequences. *Bull. Seismol. Soc. Am.* **72**, 1663–1676.
6. Davis SD, Frohlich C. 1991 Single-link cluster analysis, synthetic earthquake catalogues, and aftershock identification. *Geophys. J. Int.* **104**, 289–306. (doi:10.1111/j.1365-246X.1991.tb02512.x)
7. Molchan G, Dmitrieva O. 1992 Aftershock identification: methods and new approaches. *Geophys. J. Int.* **109**, 501–516. (doi:10.1111/j.1365-246X.1992.tb00113.x)
8. Abe S, Suzuki N. 2004 Scale-free network of earthquakes. *Europhys. Lett.* **65**, 581. (doi:10.1209/epl/i2003-10108-1)
9. Abe S, Suzuki N. 2006 Complex-network description of seismicity. *Nonlinear Process. Geophys.* **13**, 145–150. (doi:10.5194/npg-13-145-2006)
10. Baiesi M, Paczuski M. 2004 Scale-free networks of earthquakes and aftershocks. *Phys. Rev. E* **69**, 066106. (doi:10.1103/PhysRevE.69.066106)
11. Zaliapin I, Gabrielov A, Keilis-Borok V, Wong H. 2008 Clustering analysis of seismicity and aftershock identification. *Phys. Rev. Lett.* **101**, 018501. (doi:10.1103/PhysRevLett.101.018501)
12. Gu C, Schumann AY, Baiesi M, Davidsen J. 2013 Triggering cascades and statistical properties of aftershocks. *J. Geophys. Res. Solid Earth* **118**, 4278–4295. (doi:10.1002/jgrb.50306)
13. Zaliapin I, Ben-Zion Y. 2013 Earthquake clusters in southern california I: Identification and stability. *J. Geophys. Res. Solid Earth* **118**, 2847–2864. (doi:10.1002/jgrb.50179)
14. Zaliapin I, Ben-Zion Y. 2016 A global classification and characterization of earthquake clusters. *Geophys. J. Int.* **207**, 608–634. (doi:10.1093/gji/ggw300)
15. Moradpour J, Hainzl S, Davidsen J. 2014 Nontrivial decay of aftershock density with distance in southern california. *J. Geophys. Res.: Solid Earth* **119**, 5518–5535. (doi:10.1002/2014JB010940)
16. Zhang Q, Shearer PM. 2016 A new method to identify earthquake swarms applied to seismicity near the San Jacinto Fault, California. *Geophys. J. Int.* **205**, 995–1005. (doi:10.1093/gji/ggw073)
17. Benzi R, Kumar P, Toschi F, Trampert J. 2016 Earthquake statistics and plastic events in soft-glassy materials. *Geophys. J. Int.* **207**, 1667–1674. (doi:10.1093/gji/ggw366)
18. Benzi R, Sbragaglia M, Succi S, Bernaschi M, Chibbaro S. 2009 Mesoscopic lattice Boltzmann modeling of soft-glassy systems: theory and simulations. *J. Chem. Phys.* **131**, 104903. (doi:10.1063/1.3216105)
19. Benzi R, Bernaschi M, Sbragaglia M, Succi S. 2010 Herschel-bulkley rheology from lattice kinetic theory of soft glassy materials. *Europhys. Lett.* **91**, 14003. (doi:10.1209/0295-5075/91/14003)
20. Benzi R, Sbragaglia M, Perlekar P, Bernaschi M, Succi S, Toschi F. 2014 Direct evidence of plastic events and dynamic heterogeneities in soft-glasses. *Soft Matter* **10**, 4615–4624. (doi:10.1039/c4sm00348a)

21. Pelusi F, Sbragaglia M, Benzi R. 2019 Avalanche statistics during coarsening dynamics. *Soft Matter* **15**, 4518–4524. (doi:10.1039/C9SM00332K)
22. Manning ML, Liu AJ. 2011 Vibrational modes identify soft spots in a sheared disordered packing. *Phys. Rev. Lett.* **107**, 108302. (doi:10.1103/PhysRevLett.107.108302)
23. Ding J, Patinet S, Falk ML, Cheng Y, Ma E. 2014 Soft spots and their structural signature in a metallic glass. *Proc. Natl Acad. Sci. USA* **111**, 14 052–14 056. (doi:10.1073/pnas.1412095111)
24. Schoenholz SS, Cubuk ED, Sussman DM, Kaxiras E, Liu AJ. 2016 A structural approach to relaxation in glassy liquids. *Nat. Phys.* **12**, 469. (doi:10.1038/nphys3644)
25. Falk ML, Langer JS. 1998 Dynamics of viscoplastic deformation in amorphous solids. *Phys. Rev. E* **57**, 7192. (doi:10.1103/PhysRevE.57.7192)
26. Falk ML, Langer JS. 2011 Deformation and failure of amorphous, solidlike materials. *Annu. Rev. Condens. Matter Phys.* **2**, 353–373. (doi:10.1146/annurev-conmatphys-062910-140452)
27. Kapitza PL. 1951 A pendulum with oscillating suspension. *Usp. Fiz. Nauk.* **44**, 7–20. (doi:10.3367/UFNr.0044.195105b.0007)
28. Landau L, Lifshitz E 1960 *Course of theoretical physics*, vol. 1. Mechanics. New York, NY: Oxford.
29. Shishkina E, Blekhman I, Cartmell M, Gavrilov S. 2008 Application of the method of direct separation of motions to the parametric stabilization of an elastic wire. *Nonlinear Dyn.* **54**, 313–331. (doi:10.1007/s11071-008-9331-9)
30. Ramachandran R, Nosonovsky M. 2014 Vibro-levitation and inverted pendulum: parametric resonance in vibrating droplets and soft materials. *Soft Matter* **10**, 4633–4639. (doi:10.1039/C4SM00265B)
31. Benzi R, Sbragaglia M, Bernaschi M, Succi S, Toschi F. 2016 Cooperativity flows and shear-bandings: a statistical field theory approach. *Soft Matter* **12**, 514–530. (doi:10.1039/C5SM01862E)
32. Otsu N. 1979 A threshold selection method from gray-level histograms. *IEEE Trans. Sys. Man. Cyber.* **9**, 62–66. (doi:10.1109/TSMC.1979.4310076)
33. Fishkin KP, Barsky BA. 1984 A family of new algorithms for soft filling. In *ACM SIGGRAPH computer graphics*, pp. 235–244, vol. 18. New York, NY: ACM.
34. Imai H, Iri M, Murota K. 1985 Voronoi diagram in the Laguerre geometry and its applications. *SIAM J. Comput.* **14**, 93–105. (doi:10.1137/0214006)
35. Hagberg A, Swart P, Chult DS. 2008 *Exploring network structure, dynamics, and function using networkx*. Technical report. Los Alamos, NM: Los Alamos National Lab (LANL).